Facility Pressure Effects on a Hall Thruster with an External Cathode, I: Numerical Simulations

Alejandro Lopez Ortega[1], Ioannis G. Mikellides[2], Vernon H. Chaplin[3], and John Steven Snyder[4]
Jet Propulsion Laboratory, California Institute of Technology, Pasadena, CA, 91109, United States

Giovanni Lenguito[5]
Maxar, Palo Alto, California, CA, 94303, United States

Abstract: We employ the 2-D (r-z) code Hall2De to conduct numerical simulations of the SPT-140, a Hall thruster that operates with an external hollow cathode. The simulations are informed by direct measurements of the plasma conditions in the acceleration channel that were obtained using the laser-induced fluorescence technique. We validate our simulation results with additional plasma measurements, wear test erosion rates, and performance data as a function of background pressure. The comparisons of the simulation results with thrust measurements provide insight into the longstanding question of how background pressure affects Hall thruster performance. We find that in thrusters with an external cathode changes in the thrust with varying backpressure can be partially explained by changes in the plasma density near the cathode. We argue that such changes in the density affect the voltage coupling and, eventually, the thrust. However, accounting for this mechanism alone in the simulations over-predicts the thrust measured during ground tests for backpressures less than 10 μTorr. Also, at these backpressures, the measurements showed a higher rate of change of the thrust compared to the simulations. We propose that one explanation for this discrepancy is that the acceleration region may be axially shifting downstream with decreasing backpressure. Though possible, we also recognize that such shifts are not observed in LIF measurements at the lowest pressures for which such diagnostics are possible. We discuss alternative explanations in Part II of this article.

I. Introduction

Hall thrusters with externally mounted cathodes are especially prone to performance changes when the pressure of the ground facility is varied. This effect has been reported in many investigations [1-7] most of which have been experimental. Modern Hall thruster designs, such as the H6 [5] or HERMeS [8] feature centrally mounted cathodes, which have been shown to be less sensitive to background pressure effects than those with externally mounted cathodes [5]. Since at this moment there is no Hall thruster with a centrally mounted cathode qualified for flight, the incomplete understanding of the risks associated with performance dependence on facility pressure for Hall thrusters with externally mounted cathodes potentially puts constraints on the margins for science missions that will use this technology.

One prime example of this is the Psyche mission [9-10], planned under NASA's Discovery program to explore the unique metallic asteroid Psyche. The Psyche mission would be NASA's first to employ Hall thrusters, provided as a part of the solar electric propulsion (SEP) chassis from commercial partner Maxar (formerly SSL). The SPT-140 [11-13] is a mid-power class Hall Thruster that is produced by Fakel EDB (Kaliningrad, Russia). It was originally developed in the 1990's and qualified for geostationary communication satellite missions. Its current version was qualified in 2016. Maxar flew the first two flight sets (8 thrusters) in 2018, completing also a partial electric orbit

[1]Member of the Technical Staff, Electric Propulsion Group, 4800 Oak Grove Drive, Pasadena, CA, 91109, Mail Stop 125-109
[2]Principal Engineer, Electric Propulsion Group, 4800 Oak Grove Drive, Pasadena, CA, 91109, Mail Stop 125-109
[3]Member of the Technical Staff, Electric Propulsion Group, 4800 Oak Grove Drive, Pasadena, CA, 91109, Mail Stop 125-109
[4]Senior Engineer, Electric Propulsion Group, 4800 Oak Grove Drive, Pasadena, CA, 91109, Mail Stop 125-109
[5]Propulsion Development Engineer, Propulsion Group, 3825 Fabian Way, Palo Alto, CA, 94303

raising and accumulating already several thousand hours of operation. The thrusters proved the stable operation in the qualified power range from 3.0 to 4.5 kW without any off-nominal operation. Prior to selection of the Psyche mission, a series of detailed tests were performed to examine the performance, operability, and lifetime of the SPT-140 over a range of conditions and scenarios applicable to deep-space missions. The first test program investigated the performance and operation of the Development Model 4 (DM4) thruster at discharge powers of 0.23 kW to 6.0 kW, and observed stable operation and performance over this range [14]. The second test program repeated many of the same measurements on the flight-model Qualification Model 2 (QM002) thruster with similar results [15]. Recently, a study was carried out to examine the effects of facility background pressure on thruster performance [1] with the aim of predicting thrust in vacuum conditions. This study showed a higher degree of thrust sensitivity with background pressure at the high power setting of 4.5 kW. This operating condition is of key relevance to the Psyche mission as it constitutes a large portion of the cruise operations [1].

We present a numerical investigation of the effects of vacuum facility backpressure on the performance and life of Hall thrusters using the SPT-140 as a benchmark. We employ Hall2De [16-17], a 2-D axisymmetric (r-z) scientific code that has been used in the past to investigate performance [18-21] and erosion rates [18-24] of multiple Hall thrusters including the H6 [18, 20, 21, 24], HERMeS [23], and the XR-5 (formerly, the BPT-4000) [19, 22]. Hall2De was also employed in the development and demonstration of magnetic shielding [19]. The code includes a first-principles algorithm to model the effect of background neutrals and incorporates sputtering yield models of multiple materials [21, 24] that can be used to predict erosion of the thruster surfaces. While the code assumes symmetry of plasma variables around the thruster centerline, it has been used to simulate Hall thrusters with externally mounted cathodes using geometry-based approximations about the cathode plasma distribution around the thruster. A more complete description of Hall2De is provided in Section II and in [16-17]. Section II also includes a discussion on the code validation with the assistance of laser-induced fluorescence (LIF) [25, 26] measurements and the models that are employed to determine the secondary electron emission and sputtering yield of the thruster walls. In Section III, we compare the code predictions of thrust as a function of background pressure with experimental results [1]. We also provide a hypothesis about a mechanism that may be driving the well-observed non-linear variation of thrust with varying facility background gas at the lowest backpressures. We use the numerical simulations results of this section to develop a theoretical model of the thrust in our companion article and provide a second hypothesis for the thrust dependence on backpressure [27]. We argue that either one or both may be acting during pressure changes in ground testing. In Section IV, we make use of the extrapolation of Hall2De simulations to vacuum conditions to predict performance in space. Section V provides concluding remarks.

II. Computational method and comparisons with experimental measurements

A. General description of Hall2De

Hall2De is a 2-D axisymmetric code for the simulation of the plasma discharge in Hall thrusters whose development began about a decade ago. Its most notable features are described here whilst the interested reader can find the specifics of the numerical implementation in [16-17]. In Hall2De, a quadrilateral-based computational grid aligned with the magnetic field is employed. A typical simulation domain comprises the acceleration channel and a region of the plume that extends several times the length of the channel in the radial and axial directions (Fig. 1). Cylindrical geometry is assumed, with the axis being the thruster centerline, in a way such that equations of motion are only solved in the radial and axial directions (r-z). The location of the cathode is captured in the computational domain (Fig. 1). In the case of thrusters with externally mounted cathodes, such as the SPT-140, the cathode is approximated as a ring around the thruster's axis of symmetry whose inner and outer radius are defined by the distance to the thruster centerline of the inner and outer edges of the keeper orifice of the cathode. This approximation averages the distributions of the plasma properties in the vicinity of the cathode, which likely depend on z, r, and the azimuthal component θ, to a distribution with only radial and axial components. In our companion article [27], we introduce the hypothesis that the described averaging process may be responsible for some of the discrepancies observed between simulation and experimental results at very low background pressures.

The motion of each of the species in the plasma is solved separately. The density and velocity field of neutral particles is modeled assuming free-molecular flow, using a view-factor algorithm described in [28]. The presence of background neutrals is modeled as a half-sided inflow of neutral Xe atoms at the free boundaries of the computational domain. Ions are modeled using multi-fluid hydrodynamics. In [24], we made use of a hybrid hydrodynamics and particle-in-cell (PIC) approach for tracking the multiple ion populations present in the plasma according to their energy. The latter approach was motivated by the fact that in [24] the main objective was to determine the sputtering of the pole covers, which could be produced by a distribution of ions with a wide variety of energy values. However,

in the simulations presented in this work, we focus on performance and erosion of the channel walls, phenomena that is largely driven by ions generated inside the acceleration channel. These ions are always modeled using hydrodynamics equations in Hall2De since, as it was shown in [16-17], ions generated in the channel have sufficiently long residence time compared to their collision time to warrant a Maxwellian distribution. Our SPT-140 simulations are then run assuming two fluid populations, with the threshold between populations being 150 V. The second ion population comprises ions generated in the plume, which have very low velocity compared to the beam ions (i.e., ions generated inside the acceleration channel) and do not equilibrate with them. Separate continuity and momentum equations are solved for each fluid population, *iF*, and each charge state, *iC*. Ions of different *iF* and *iC* numbers can interact with one another through ionization, charge exchange, and elastic collisions.

Electron motion is modeled using a fluid approach where inertia is neglected. This approach results in a vector form of Ohm's law that is solved in the directions parallel and perpendicular to the magnetic field lines and enables computation of the plasma potential when combined with current conservation and the assumption of plasma quasi-neutrality. Electron temperature is determined as the solution of an energy conservation equation.

Boundary conditions are imposed as follows. The channel walls and pole surfaces are modeled as insulators and the sheath that develops is computed based on the Hobbs and Wesson solution to the 1-D sheath equations, accounting for secondary electron emission [29]. There is some variation of the secondary electron emissions models depending on the grade of boron nitride employed. We discuss the effect of the secondary electron emission model on erosion of the channel walls and performance in Section II D. The anode walls and pole covers are modeled as conductors at fixed voltage. We also specify the neutral flow rate across the injection area of the anode. At the cathode boundary, we specify electron temperature, plasma potential and mass flow rate of neutrals and ions.

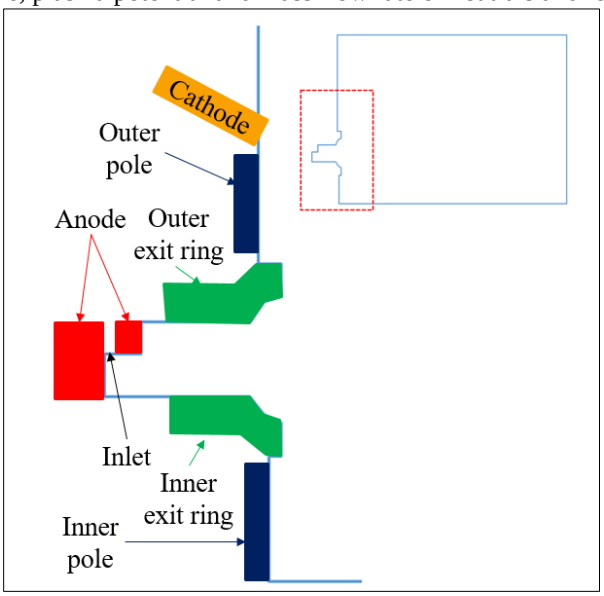

Fig. 1: Hall2De computational domain (top-right) and schematic of the thruster geometry

B. Operating conditions and input parameters

We investigate four operating conditions of the SPT-140 at power levels of 4.5, 2.5 and 1.0 kW. The discharge voltage is fixed at 300 V. Two conditions at 4.5 kW are considered, with magnet currents of 5.25 A and 6 A. The magnet current determines the strength of the magnetic field, with a linear correlation existing between the two. The was used in the long duration (>10,000 h) wear test of the SPT-140. The latter was selected as part of mission profile of the Psyche mission as it yields a higher thrust to power ratio (see Fig. 8). The results of these simulations are compared with the results of laser-induced fluorescence measurements of the ion velocity distribution at the centerline of the channel, performed at multiple background pressures. The mass flow rate in the simulations is adjusted to match that of the experiment for each background pressure measurement. The exact operating conditions at vacuum (i.e., mass flow rate) are not available and we employed the same input parameters of the lowest background pressure available. The cathode flow rate also mimics the tests. The nominal rate is 5% of the anode flow rate except for the 1.0 kW condition, which uses 9% of the anode flow rate. The conditions at the cathode exit were estimated from separate simulations of the SPT-140 cathode using the 2-D axisymmetric Orificed Cathode (OrCa2D) code [30-36].

The plasma potential at the cathode exit makes use of the cathode-to-ground voltage obtained during tests, which remains largely insensitive to the background pressure.

Table I. Input parameters for SPT-140 simulations

Discharge power (kW)	Magnet current (A)	Discharge voltage (V)	Anode mass flow rate (mg/s) (Background pressure (μTorr))					Electron temperature at cathode exit (eV)	Plasma potential at cathode exit (V)	Cathode flow rate (% of anode flow rate)
4.5	6.0	300		14.97 (30)	15.00 (15)	14.95 (9)	14.95 (0)	4.0	20.4	5
4.5	5.25	300	*14.5 (59.2)	14.58 (30)	14.50 (15)	14.48 (9)	14.48 (0)	4.0	17.0	5
2.5	4.0	300		9.1 (30)		9.1 (6)	9.1 (0)	4.0	19.9	5
1.0	2.75	300		3.9 (30)		4.27 (2.9)	4.27 (0)	4.0	26.0	9

*Conditions of long duration life test. No LIF measurement at this background pressure. Mass flow rate from long duration life test data

C. **Numerical simulation results**

A first-principles closure model for the anomalous transport of electrons across magnetic field lines in Hall thrusters remains elusive today. Thus, in Hall2De closure is achieved through an anomalous collision frequency that is derived empirically. Its spatial profile in the r-z domain is for a given operating condition based on experimental measurements. These include global metrics such as discharge current as well as spatially-resolved local plasma parameters including electron temperature and ion velocity. For this study, we adopted the spatial evolution of this latter parameter, the ion drift velocity along channel centerline, as the primary experimental measurements for informing the anomalous collision frequency in Hall2De. We employed a non-resonant laser induced fluorescence diagnostic to characterize this plasma property [25-26]. In brief, this non-resonant LIF scheme relies on inducing a transition in a metastable state of Xe II singly charged ions with injected light from a tunable diode laser. By scanning the laser wavelength across this metastable transition and monitoring the intensity of the fluoresced signal, it is possible to infer the Doppler broadening in this transition state that is the result of ion motion. This in turn leads to an assessment of the local ion velocity distribution function (IVDF). The system we employed for this work yielded IVDFs with a spatial resolution of 2 mm. The values for ion velocity reported here were found by taking the first moments of the measured IVDFs.

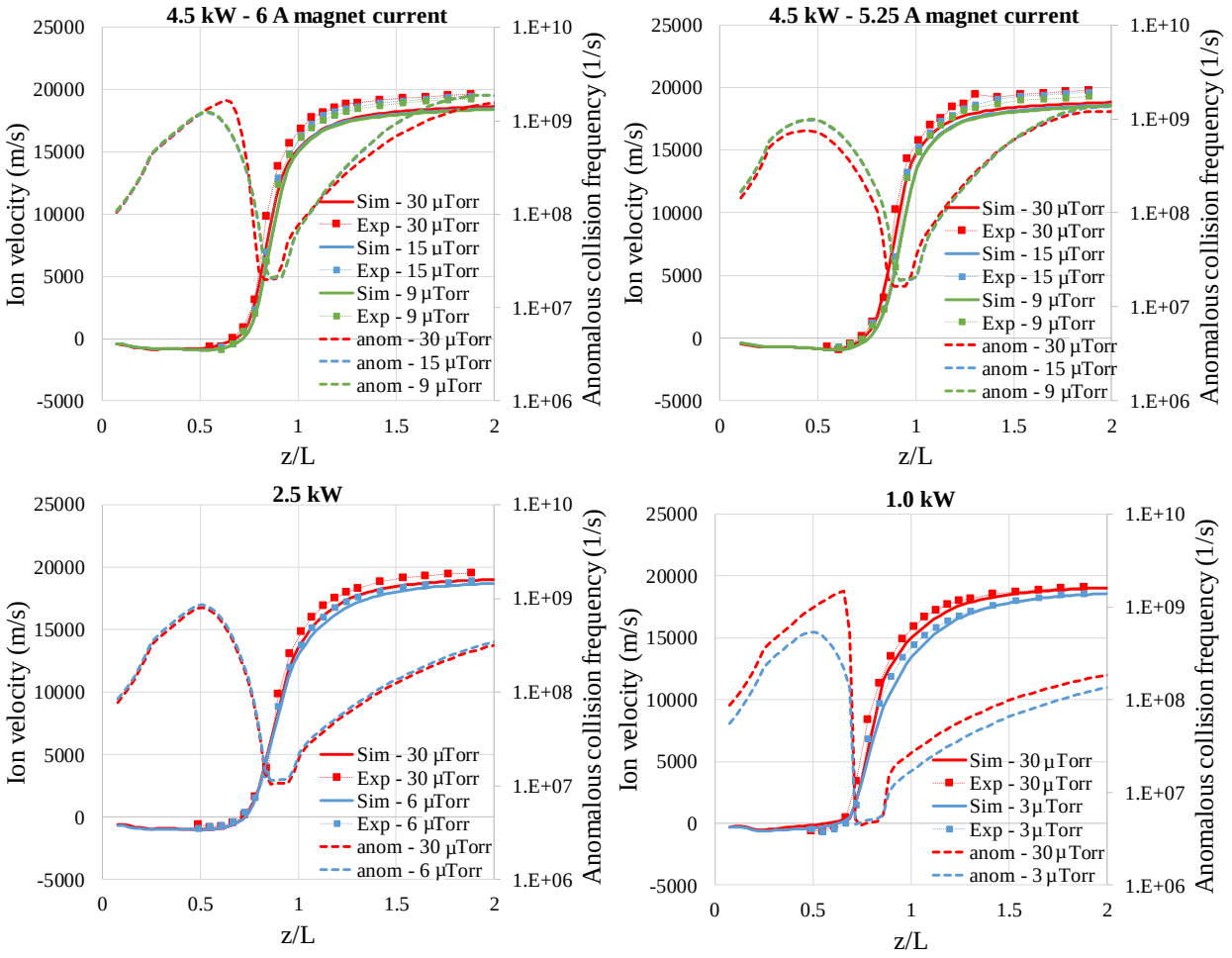

Fig. 2: Comparison between ion velocity at the channel centerline from simulations and LIF measurements for all operating conditions and background pressures for which LIF measurements were available. Anomalous collision frequency distribution employed is predicted in the simulation in dashed lines.

Figure 2 depicts a direct comparison of the ion velocity between the simulations and the LIF measurements at the channel centerline. L is the acceleration channel length, with z/L=0 and z/L=1 at the anode and channel exit, respectively. We also present the anomalous collision frequency profiles that were employed in the simulations. These profiles were modified iteratively for each specific simulation (operating condition at a given background pressure) until the numerical solutions agreed well with the LIF measurements. We discuss here some important conclusions that can be extracted from the comparisons in Fig. 2. First, one leading argument to explain the degradation in thrust at lower background pressures is that the acceleration region moves downstream (away from the anode). While we observe some downstream motion of the acceleration region at lower background pressure (most clearly for the 1.0 kW and 4.5 kW – 5.25 A magnet current conditions), this shift is very small (less than 5% of the acceleration channel length). That is, the largest shifts appear to occur at the higher pressures and diminish as the pressured is lowered. It is possible that the downstream motion only occurs for extremely small background pressures but the reasons such behavior would occur is unclear. Also, measurements in this range of pressures were not possible. We also notice that changes in the anomalous collision frequency profile as a function of background pressure are extremely small, especially under the light of the results presented in [37], which suggested that large changes in the anomalous collision frequency in the interior of the acceleration region only result in variations of the plasma parameters that are within the uncertainty of the experimental measurements. The second conclusion is that the ion velocity downstream of the acceleration region increases at higher background pressures. The latter means that the beam is subject to a larger electric field at higher background pressure, which in turn leads to higher thrust due to an increased voltage utilization

efficiency. This mechanism can explain part of the thrust dependency on background pressure and will be discussed in more detail in Subection III B.

We conclude this subsection, by providing additional comparisons between the simulations and laboratory data. In Fig. 3, we depict the LIF measurements at the edges of the beam obtained for the 4.5 kW – 6 A magnet current operating condition at 30 μTorr superimposed with ion velocity vectors extracted from the corresponding simulation. The scale used for the vector magnitude is the same for both sets of data. We observe that the agreement in both direction and magnitude is excellent. We found that the simulation results at other operating conditions display similar levels of agreement with the measurements.

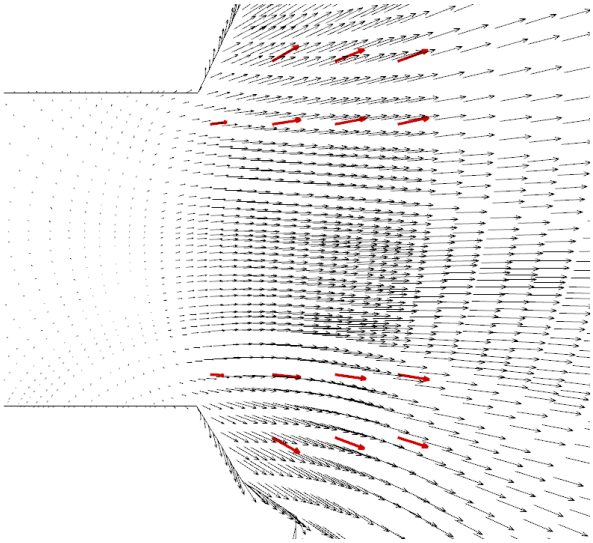

Fig. 3: Ion velocity vectors at the edges of the beam extracted from LIF measurements (red) and superimposed to velocity vector field obtained from Hall2De simulation (plotted at each computational cell) of the SPT-140 at 4.5 kW – 6 A magnet current and 30 μTorr.

D. Sputtering yield model for boron nitride channel walls

The erosion model in Hall2De is described in detail in [24]. Succinctly, we compute at each time-step of the simulation the erosion produced by each ion population (iF, iC) as a function of the ion current density and velocity vector near the walls. The total erosion rate at each location is computed as the aggregate of the contributions to the erosion of all the ion populations divided by the simulation time. The sputtering yield is modeled as the product of the angular yield (i.e., the effect of the angle of incidence for fixed kinetic energy) and the energy yield, which depends only on the ion kinetic energy. Because ions must traverse a sheath before striking the wall, the total impact energy is the sum of the kinetic energy ions have acquired in the plasma upon entrance to the sheath, and the sheath potential energy. For the latter, we make use of the potential energy, transformed to ion kinetic energy as the plasma ions accelerate inside the sheath towards the solid material [29]. The angular dependence implemented in Hall2De is described in [24]. Variations of the angular yield within the uncertainty of the measurements for the incidence angles found in the channel do not have a significant effect on the predicted erosion. The energy yield follows Bohdansky equation [38]

$$f_{K,iC}(K) = \frac{A}{iC}\left(1-\frac{E_T}{E}\right)^2\left(1-\left(\frac{E_T}{E}\right)^{\frac{2}{3}}\right), \quad (1)$$

In a previous article [21], we argued that the values of the coefficients A and E_T in (1) have a large degree of uncertainty due to the lack of measurements below 100 V [39]. We estimated in [21] that $20<E_T<50$ V, a value that can also vary with the grade of boron nitride employed. As will be shown in Fig. 6, the values for "Model 2" in Table II, which result in a close agreement to the experimental data of Yalin et al. [39] (Fig. 4) produce a reasonably good agreement with the erosion rates at beginning of life extracted from the long duration wear test. However, even better agreement with the erosion rates are achieved if "Model 1" is employed. Model 1 predicts slightly lower erosion rates than "Model 1" for ion energy values above 80 V. Note that the value of E_T in "Model 1" is within the uncertainty range estimated in [21].

Table II. Coefficients in Bohdansky equation for sputtering yield models 1 and 2

Model	A (mm^3/C)	E_T (eV)
1	0.015	25
2	0.035	35

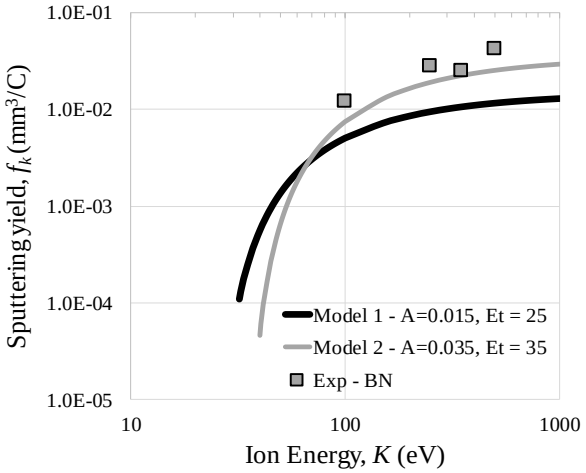

Fig. 4. Left: Sputtering yield for perpendicular xenon ion bombardment on boron nitride (BN). Comparison between Models 1 and 2 (Eq. (1) and Table II) and experimental data [39].

The secondary electron yield model of boron nitride also affects the erosion rate as it determines the sheath potential, which accelerates ions beyond their pre-sheath velocity. As implemented in Hall2De, the secondary electron yield takes the expression

$$Y_{SEE} = \min\left(0.983, Y_0 + 2(1 - Y_0)\frac{T_e}{E_1}\right), \quad (2)$$

where 0.983 is Hobbs and Wesson's limit for an electron repelling sheath [29] and Y_0 and E_1 are coefficients that represent the limit of the secondary electron yield at zero temperature and half Maxwellian cross-over, respectively. The sheath potential is computed as a function of Y_{SEE} using the polynomial fit described in [40]. We include in our discussion two different set of values for the coefficients in Y_{SEE}. "Model 1" has been used in Hall2De since 2011 and was calibrated with data from the BPT-4000 thruster [19]. "Model 2" is based on a fit to the data published by Raitses et al. [41] for the boron nitride in the SPT-140 at high temperature. A graphic comparison between the two models in shown in Fig. 5

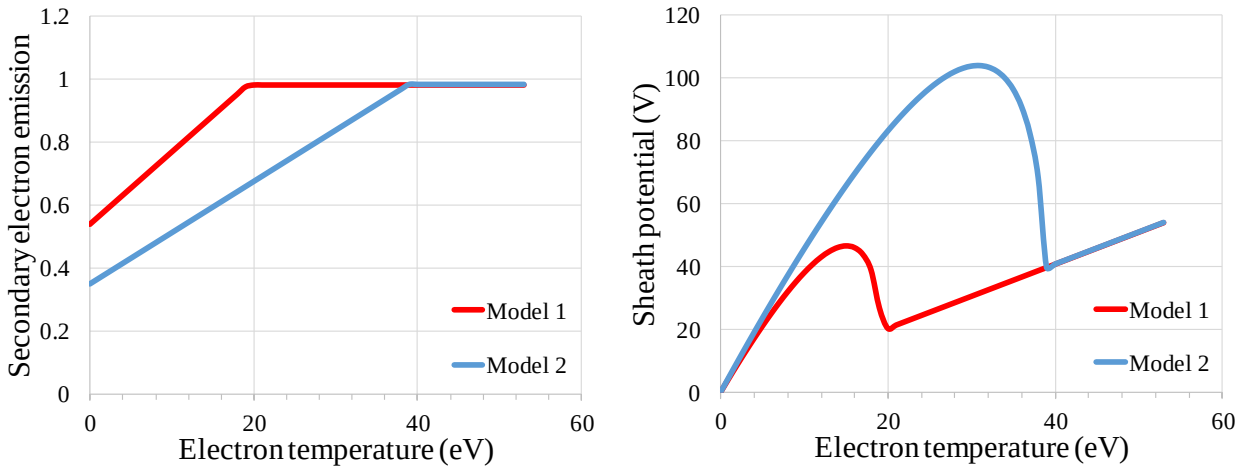

Fig. 5: Secondary electron emission (left) and sheath potential (right) for boron nitride as a function of electron temperature (eV) for models 1 and 2.

Table III. Values of Y_0 and E_1 used in sputtering yield models 1 and 2

Model	Y_0	E_1 (eV)
1	0.54	40
2	0.35	80

We make use of the SPT-140 wear test results at beginning of life to determine how erosion rates computed from simulations using the two models presented above compare with experimental data. The measured erosion rates are derived from the comparison between the geometry of the channel rings after 190 and 529 h of test with respect to the initial geometry. The data at 190 h is less reliable than that for 529 h as the former shows no erosion for some large portions of the inner ring between z/L=0.9 and z/L=1, which can likely be attributed to initial carbon deposition on this surface. Our simulations show that it is impossible to achieve a zero-erosion state at that particular location of the thruster. The numerical simulations make use of the operating conditions described in Table I. However, we must note that no LIF measurements were available at the exact background pressure of the wear test facility. To circumvent this difficulty, we employed the anomalous collision frequency distribution for the simulation at 30 μTorr, making the assumption that the acceleration region will not move significantly between 30 and 59.2 μTorr. We have a high degree of confidence that this assumption is not far from reality as the thrust predicted by the simulation at 59.2 μTorr is in close agreement to its experimental value as is the simulation at 30 μTorr (see Fig. 8).

The erosion rates predicted by the combination of the four models described below, compared with the wear test results, are shown in Fig. 6. All the models are within a factor of two of the measured values between z/L=0.9 and z/L=1. However, the sputtering yield "model 1" produces more accurate results due to its lower coefficient A. The main difference between models occurs at predicting the erosion rates upstream of z/L=0.9. "Model 1" for the sputtering yield also produces a better agreement with the experimental measurements due to its lower E_T coefficient. E_T represents the sputtering threshold, such that ions with energy values below E_T produce negligible erosion. Since the energy of the ions increases as they move along the acceleration channel, a lower E_T will move upstream the location at which the erosion of the channel starts. This location moves even more upstream when "Model 2" for the secondary electron emission is employed. The latter is because, at a given temperature, "Model 2" predicts a larger sheath potential and thus ions gain additional kinetic energy as they traverse the sheath. Error analysis with respect to the experimental measurements reveals that the combination of "Model 1" for the sputtering yield and "Model 2" for the secondary electron emission lead to the most accurate erosion rate predictions. These two models will be used in all the simulations presented hereinafter. We note that thruster performance for the four simulations presented here was the same, with the thrust varying at most by 1 mN between simulations.

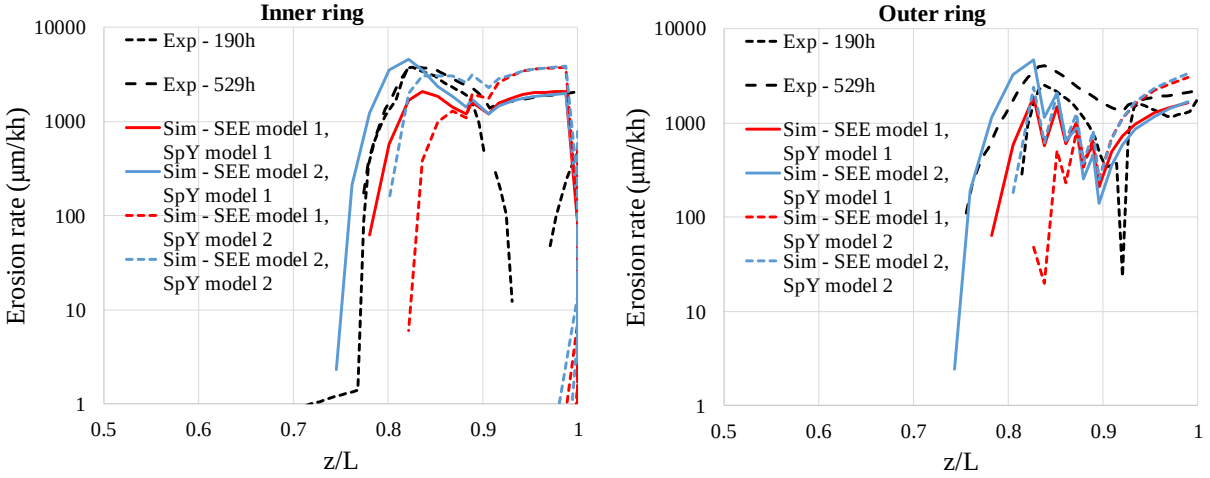

Fig. 6: Comparison of predicted erosion rates (Hall2De) and wear test results for the sputtering yield (SpY) and secondary electron emission (SEE) models described in Tables II and III. Operating conditions are beginning of life, 4.5 kW, 5.25 A magnet current and background pressure of 59.2 μTorr.

We have shown that our simulation results compare well with the measured erosion rates of the life test at the beginning of life within the uncertainty range of the boron nitride models for secondary emission and sputtering rate.

We conduct additional validation of our numerical solution and boron nitride models by computing a new geometry for the channel at the same time intervals reported in the wear test. The eroded geometry (extracted by integration of the erosion rate values over time) is employed in a new simulation with equal initial parameters to the beginning-of-life simulation (Table I). This iterative process, carried out to replicate the state of the thruster after 190, 529, 1253, and 1630 h of operation during the wear test, is depicted in Fig. 7 and allows us to compare the thruster geometry during the life test with its numerical replica. We observe that our estimates of the exit rings geometry as a function of time are in excellent agreement with the measured geometry.

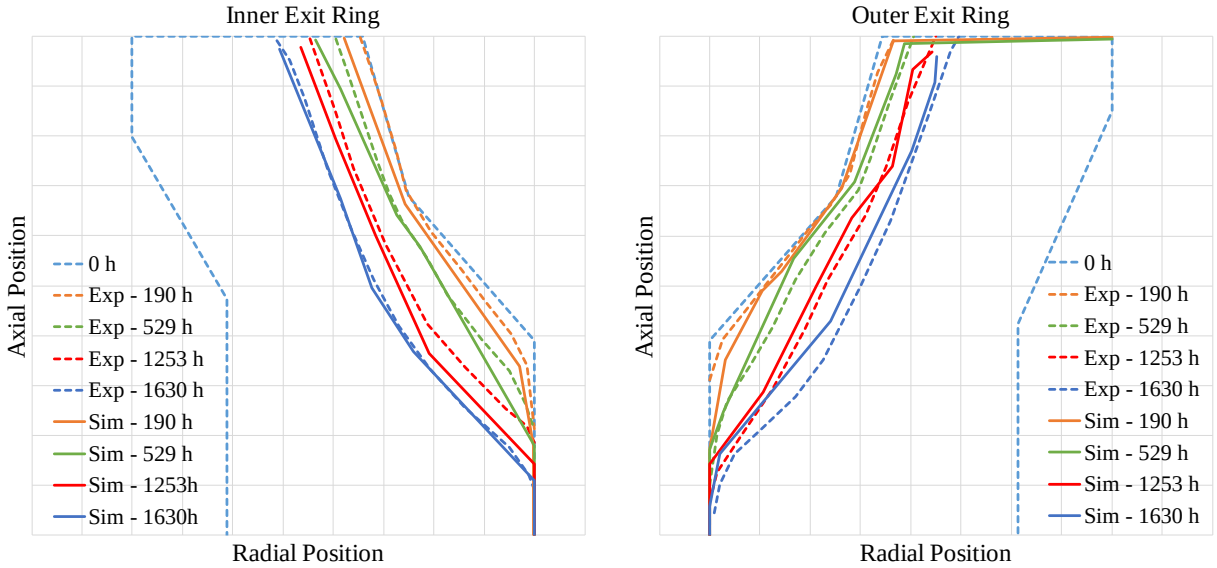

Fig. 7: Comparison of predicted erosion as a function of time (Hall2De) and wear test results. Progressive erosion of the channel rings in the simulations closely matches the erosion profiles observed in the long duration wear test.

III. Performance trends with background pressure

A. Thrust dependence on background pressure

In this section we discuss our findings from the numerical simulations of the SPT-140 performance and its dependence on the facility backpressure. Figure 8 shows a comparison between the thrust values obtained with Hall2De and those of performance tests for the operating conditions outlined in Table I. Thrust due to charged species in Hall2De is computed by integration along each magnetic field line of the momentum flux

$$T_{Bln,ion} = m_{Xe} \sum_{j_{edg} \subset Bln} \sum_{iF} \sum_{iC} n_{iC,iF} u_{z,iC,iF} \boldsymbol{u}_{iC,iF} \cdot \widehat{\boldsymbol{n}_j} A_j, \tag{3}$$

where j_{edg} is an edge that conforms the magnetic field line, $\widehat{\boldsymbol{n}_j}$ is the normal vector to the edge surface, A_j is the area of the edge (considering it as an element of revolution around the thruster centerline), m_{Xe} is the mass of a xenon atom, and for each fluid iF and charge number iC, n, $\mathbf{u}$, and u_z represent, respectively, the density, the velocity vector, and the velocity component in the axial direction. We also account for the contribution of charge exchange neutrals to the thrust. This is done by accounting for the momentum transferred from ions to neutrals through charge exchange at a rate $\dot{n}_{CEX}$ at each cell (with volume V_j) upstream of a given magnetic field line

$$T_{Bln,CEX} = m_{Xe} \sum_{j_{cell} - upstream\ of\ Bln} \sum_{iF} \sum_{iC} \dot{n}_{CEX,iC,iF} u_{z,iC,iF} V_j. \tag{4}$$

The total thrust $T_{Bln} = T_{Bln,ion} + T_{Bln,CEX}$ is evaluated at each magnetic field line and the maximum value $T = max_{Bln} T_{Bln}$ is reported as the computed thrust in the simulation.

We comment first on the background pressure range for which LIF measurements exist. At 4.5 kW, this range is from 9 to 30 μTorr. For the 6-A magnet current operating condition, the simulation results are within the experimental uncertainty of the measurements. It is worth noting that that simulations at 9 and 15 μTorr (and also the simulations at lower background pressures) assume no axial displacement of the anomalous collision frequency profile (Fig. 2) because the LIF measurements at these two pressures revealed negligible axial differences between the ion velocity fields along the channel centerline. Under this assumption we found that the relationship between thrust and background pressure is linear. At 30 μTorr, the anomalous collision frequency informed by LIF, as seen in Fig. 2, is larger than at lower background pressures immediately upstream of the acceleration region. It was shown in [17] that such higher values of the anomalous collision frequency in the channel lead to lower thrust for a given background pressure. Thus, the increase in thrust due to a larger background pressure is partially canceled by the changes in the anomalous collision frequency. To confirm this last result, we performed a numerical experiment (not shown here) in which we used the anomalous frequency model of the 15 μTorr case with a background pressure of 30 μTorr. The latter simulation yielded a higher thrust, the value of which correlated with the linear relationship established by the simulations for pressures <15 μTorr (see Fig. 8). In the next subsection and in our companion article [27], we discuss the physical mechanisms that affect thrust during changes in the background pressure. We also note that the computed thrust at very low background pressures (<9 μTorr) is higher than the measurements. We find two possible explanations for this discrepancy: the first is that the acceleration zone is axially displaced at very low background pressures and will be investigated in Section IV. The second is that there are non-axisymmetric effects in the vicinity of the cathode that are not captured in a 2-D axisymmetric code. We report on the latter mechanism in detail in our companion article [27]. We mention here as a summary that the azimuthal distribution of plasma and neutral density in the plume of the cathode becomes more relevant as the background pressure becomes negligible with respect to the cathode flow of neutrals. This can lead to additional changes in the plasma potential in the plume. The implications of plume potential changes on the thrust are discussed in more detail in the next subsection.

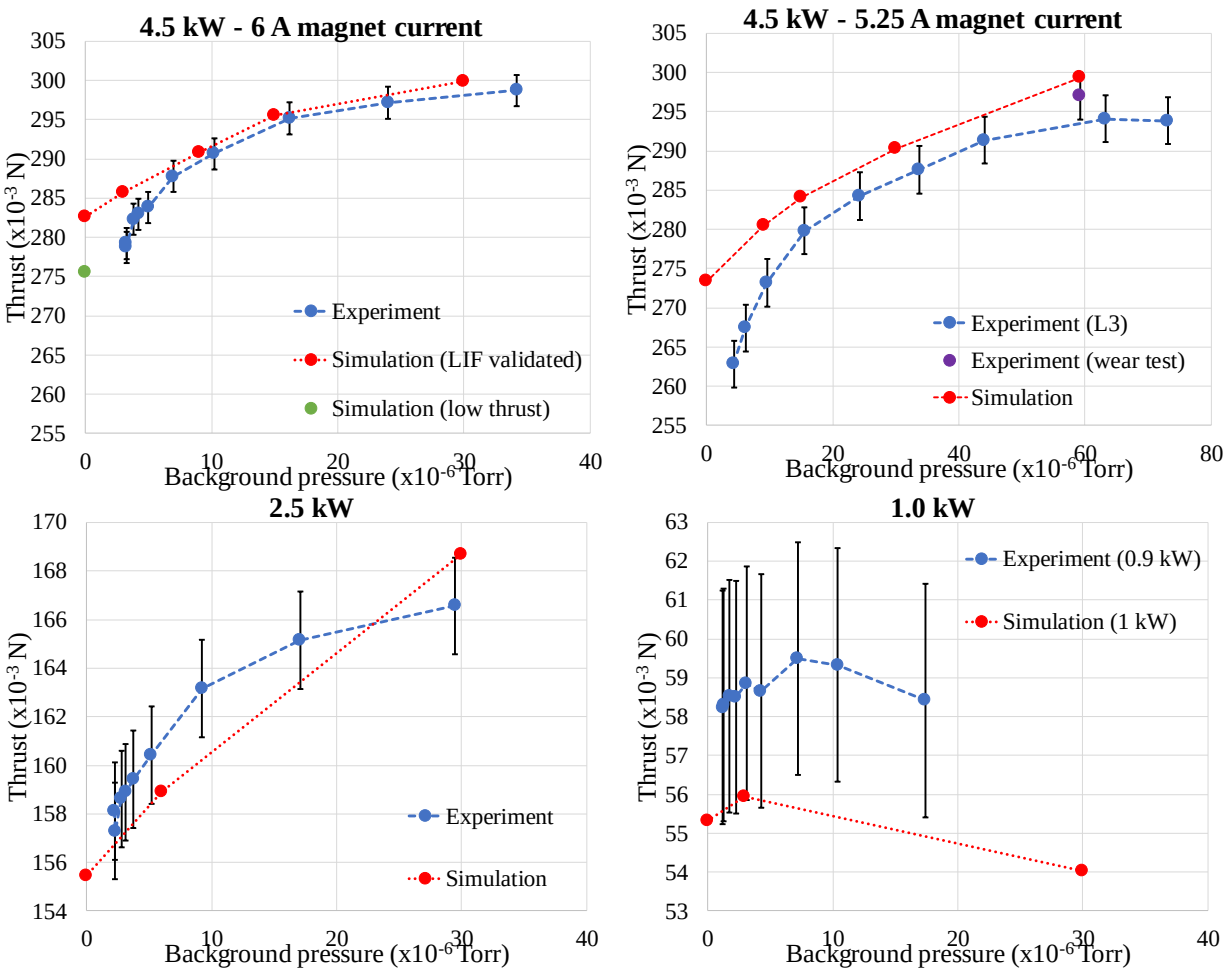

Fig. 8: Thrust vs background pressure curves for operating conditions in Table I. Comparison with experimental measurements from [1]

For the 5.25-A magnet current case, the comparisons between results and simulations are similar to those of the 6-A magnet current case. Here, we include the result of the simulation that matches the conditions of the wear test (59 μTorr) and that was described in detail in the previous section. The measurements denoted as "Experiment (L3)" in Fig. 8 were taken in a different facility than that of the wear test ("Experiment (wear test)") and the rest of measurements shown in Fig. 8. The SPT-140 thruster employed in each of the tests had also slightly different levels of wear. It is worth noting that the thrust at this operating condition decays in a steeper fashion than in the 6-A condition. This effect is discussed in detail in Section III C.

At 2.5 kW our simulations are within the experimental uncertainty. In this case, we only have LIF measurements at two background pressures, making it harder to predict the trend in thrust between 6 and 30 μTorr. However, the axial position of the ion velocity profiles from the LIF measurements at these two operating conditions (Fig. 2) was almost identical, from which we can infer that axial displacements of the anomalous collision frequency profiles are not likely. The linear trend of thrust as a function of background pressure from 0 to 30 μTorr in the simulations is consistent to what was found in the 4.5 kW – 6 A magnet current simulations because, similarly to the latter case, we made no significant modifications in the anomalous collision frequency between the low and high background pressures. The measurements however show a steeper decay of the thrust at lower background pressures. It is worth noting here that the change in the measured thrust at 2.5 kW is much smaller than at 4.5 kW (6 mN vs 13 mN between 6 and 30 μTorr). We have found that changes in the axial displacements of the anomalous collision frequency for $z/L<1$ that are small enough to keep the discrepancy between computed and measured ion velocities within the uncertainty of the LIF diagnostics can lead to changes of up to 3 mN in the computed thrust. Hence, since the anomalous frequency is empirically derived there is an experiment-based uncertainty in the numerical simulations of ±3 mN. We also found that such small changes affect negligibly the computed erosion profiles along the rings.

Finally, the 1.0-kW case does not exhibit a decay in thrust with background pressure. We note that, for this operating condition, the comparison is against the closest operating conditions for which thrust measurements were available (0.9 kW). The evolution of the plasma conditions with background pressure at 1.0 kW is not significantly different to what was observed in other operating conditions. Thus, the discussion in the next subsections is still largely valid at 1.0 kW. However, it was reported in Table I that at 1.0 kW, there was a 10% increase in the anode mass flow rate (an input in Hall2De) between 30 and 3 μTorr. We found that this was enough to compensate for the degradation in thrust with pressure since more propellant is introduced in the thruster. For all the other operating conditions, the mass flow rate was kept approximately constant as a function of background pressure (Table I).

B. Discussion on mechanisms that contribute to the thrust variation at low background pressure

One of the long-sought goals of the electric propulsion community has been to have the ability to predict thruster performance in space based on measurements made in vacuum facilities. This objective can only be achieved with a physics-based model of the thrust that accounts for all background pressure-related effects. Here, we present a summary of the most relevant changes in plasma parameters that we observed in our simulations at different background pressures at the 4.5 kW, 6 A magnet current operating condition. The conclusions of this subsection are also applicable to the other operating conditions. The insight gained from the simulations has been used to support the development of a theoretical model of the thrust in Hall thrusters and is presented in our companion article [27]. The model in [27] is then used to expand the findings from the simulations on the mechanisms that may be driving the observed dependence of thrust on facility backpressure.

Table IV summarizes the thrust as a function of background pressure and the contribution of each species (ions and neutrals) to it. The most relevant result is that the contribution of ions to the thrust appears to be constant while the contribution of neutrals increases with background pressure. The increase in thrust with background pressure due to the additional neutrals produced by charge-exchange (CEX) collisions with ions is linear, resulting in the thrust trend reported in the previous section. We term this contribution in Table IV as "CEX thrust". The observed linear trend can lead to the simplistic argument that the increase in thrust is only due to the presence of more CEX neutrals in the thruster plume as the background pressure increases. However, the bulk of neutrals that contribute to the thrust is made of ions that were generated in the channel, accelerated by the electric field, and only became neutrals due to CEX collisions in the downstream plume. Thus, the physical explanation to the thrust dependence on background pressure must be found by examining the conditions immediately downstream of the acceleration region.

Table IV. Thrust values and contribution to ions and charge-exchange neutrals to thrust as a function of background pressure for the 4.5 kW – 6 A magnet current operating condition.

Background pressure (μTorr)	Thrust (mN)	Ion thrust (mN)	CEX thrust (mN)	CEX % of total thrust
15	295.5	278.2	17.3	5.9
9	290.8	278.4	12.4	4.3
0	282.6	278.5	4.1	1.5

In Fig. 9, we depict the radial distribution of plasma potential and density for a radial profile downstream of the acceleration region for the simulations in vacuum and at 30 μTorr. The plasma density at the channel centerline ($r/R_C=1$) is the same in both cases. The plasma density at the channel centerline is largely driven by the conditions inside the channel, which are not affected by the background pressure. At $r/R_c>1$, the plasma density decreases more steeply in vacuum. This is a consequence of the lower background pressure, which in turn drives down the number density of plume ions. Since the cathode in the SPT-140 is externally located, we find that the difference in plasma potential between the cathode exit and the beam is driven by the change in plasma density along the magnetic field line that links the cathode to the beam, according to Boltzmann's law

$$\phi_2 - \phi_1 = T_e log\left(\frac{n_2}{n_1}\right), \quad (5)$$

where ϕ, T_e, and n are the plasma potential, electron temperature, and plasma density, respectively. The indexes denote two different locations and we have assumed that the magnetic field lines are isothermal (an assumption based on the results of our simulations). While the radial profile in Fig. 9 is not completely aligned with a magnetic field line and thus is not isothermal, we can argue that if we follow such a line from the $r/R_c>1$ to the $r/R_c=1$-regions, the plasma density gradient will be larger at low background pressures. Since the potential at the cathode remains approximately constant with background pressure, the consequence is that the plasma potential in vacuum at the channel centerline is higher as the background pressure decreases. Thus, the ions are accelerated to a lower potential differential at low background pressures, which leads to decreased voltage utilization efficiency and thrust. Equation (5) actually holds

along the radial profile of Fig. 9 when using an electron temperature of 5.5 eV, which is approximately the average temperature along the radial profile. The significance of Eq. (5) on thrust and its dependence on backpressure is discussed further in [27]. Finally, it is worth noting here that the LIF measurements also showed lower ion velocity in the near-plume region at low background pressures (Fig. 2).

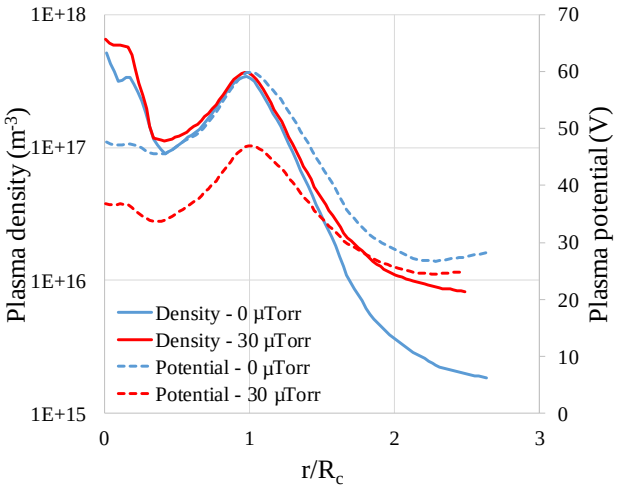

Fig. 9: Plasma density and potential distribution of a radial profile at z/L=1.7 at high (30 µTorr) and low (vacuum) background pressures. R_c is the distance between the centerline of the acceleration channel and the thruster centerline.

We conclude this section by noting that our thrust predictions are higher than the measured values at the lowest backpressures. Thus, the explanation given in this subsection related to Eq. (5) only partially captures the observed thrust variation at low background pressures. It appears therefore that additional processes must be are at play. We discuss two such processes, one in Section IV and one in [27], either or a combination of which could explain the observed trends.

C. Thrust degradation at different magnetic field strengths

In this subsection, we explain the causes for the steeper degradation of thrust at low background pressures observed for the 4.5-kW, 5.25-A magnet current operating condition with respect to the same power setting at higher magnet current. Figure 10 shows the location of the acceleration region for both 4.5-kW operating conditions at high and low background pressures (30 and 9 µTorr). We observe that for a given background pressure the acceleration region at 5.25 A of coil current is always downstream of that at 6 A. In addition, the downstream shift in location between 30 µTorr and 9 µTorr is larger at 5.25 A. Our simulations show that the more downstream the location of the acceleration region is with respect to the channel exit the lower the thrust is due to the higher beam divergence losses. Thus, in the case of the 5.25-A magnet current operating condition, we need to add the decrease in thrust due to a larger downstream shift in the acceleration region to the phenomena reported in the previous subsection. Figure 11 shows the contour plots of the ion density at 30 µTorr and 9 µTorr, which highlight changes in divergence angle due to the location of the acceleration region. We must emphasize that the physical mechanisms that dictate the location of the acceleration region are closely linked to the anomalous transport physics which remain elusive today [42, 43 and references therein] and, are therefore beyond the scope of this article.

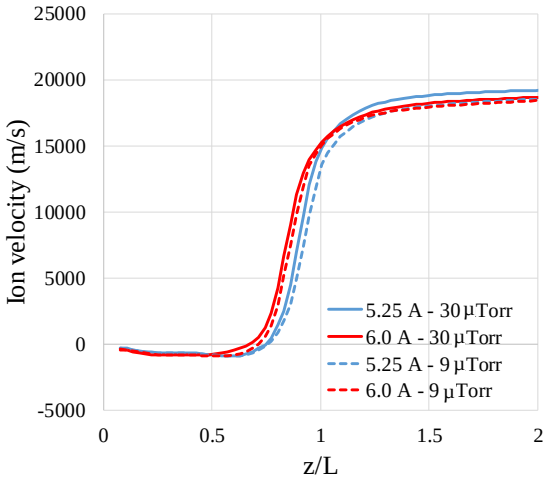

Fig. 10. Ion velocity along the channel centerline for operating conditions at 4.5 kW (5.25 A and 6.0 A magnet current) at background pressure of 9 and 30 µTorr.

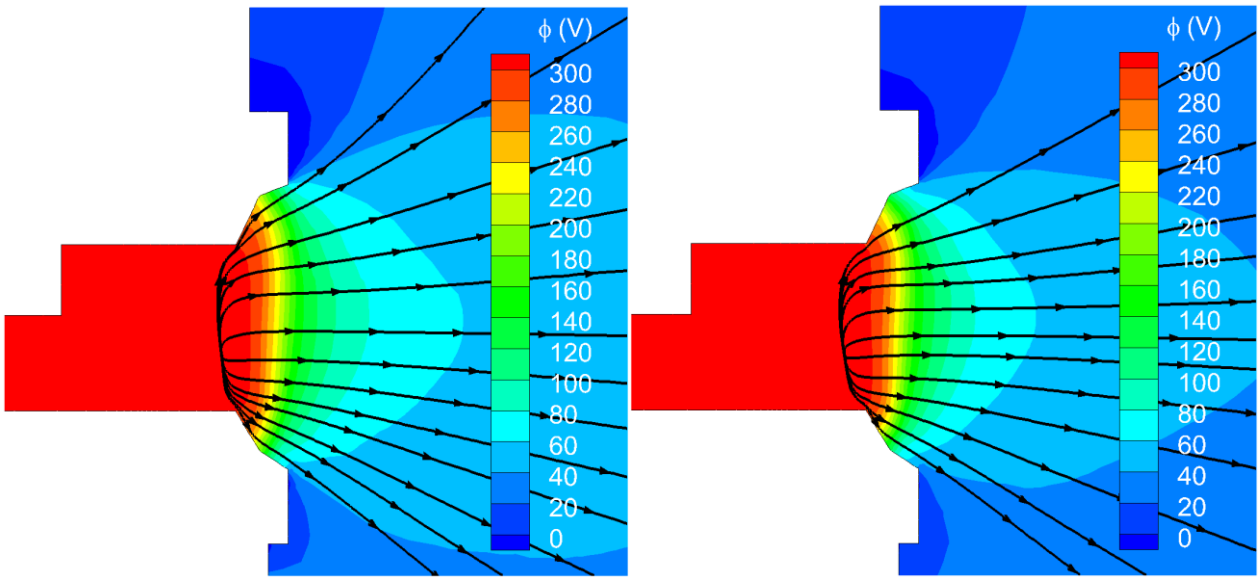

Fig. 11. Plasma potential contours for 4.5-kW, 5.25-A magnet current operating condition at 9 and 30 µTorr. The acceleration region at 5.25 A is axially located downstream of that at 6 A which leads to higher beam divergence losses and lower thrust in the former magnetic current condition.

IV. Extrapolation of results to vacuum conditions

Because performance and wear predictions in space are mission critical, we revisit in this section our simulations in vacuum. The results shown in Fig. 8 at vacuum were obtained with the same anomalous collision frequency distribution as the lowest background pressure for which LIF measurements were available. In other words, it was assumed that no axial displacement of the acceleration region occurred from these pressures to vacuum. However, as discussed briefly in Section III A, the computed thrust trend at 4.5 kW exceeds the measured thrust at the lowest background pressure for which measurements are available, which implies that our thrust prediction for vacuum also overestimates the (unknown) true value. In this subsection, we investigate the hypothesis that the change in thrust in vacuum (and background pressures below 9 µTorr) is due to additional downstream motion of the acceleration region. We must note however that no change in the acceleration region location was observed in the LIF measurements between 9 and 15 µTorr. Therefore, albeit possible, if such movement occurred at the lower pressures the reasons for it are presently unclear. An alternative explanation to the one given here for the discrepancy in thrust is found in our companion article [27]. We performed an additional simulation (termed "low thrust" in Figs. 8 and 12) in which a

downstream displacement of the acceleration region by $\Delta z/L = 0.06$ was achieved by a similar axial shift in the anomalous collision frequency profile. The location of acceleration region in this new simulation is still reasonable for two reasons. First, the downstream shift in the "low thrust" simulation is comparable to the shift observed between 30 and 15 µTorr in the 4.5 kW – 6 A magnet current operating condition. Second, the new location is comparable to the furthest downstream location found in the LIF measurements for any operating condition, which occurs for the 4.5 kW - 5.25 A magnet current condition (shown in Fig. 12 for reference). The thrust of the new simulation is 8 mN lower yielding a trend of the thrust that is in closer agreement with the measurements at very low background pressures. The comparison between the erosion rates at the channel walls produced by the original simulation and the new one are depicted in Fig. 13. We observe that the two predictions are within a factor of two in the downstream portion of the channel. As the acceleration region moves downstream in the "low thrust" simulation, the location at which significant erosion begins also moves downstream (from z/L~0.73 to z/L~0.79). The erosion rates from the wear test are also included in Fig. 13 to provide a visual cue to highlight that the erosion at 6-A of magnet current in vacuum is similar to the wear test results, which were performed with a magnet current of 5.25 A and background pressure of 59.2 µTorr.

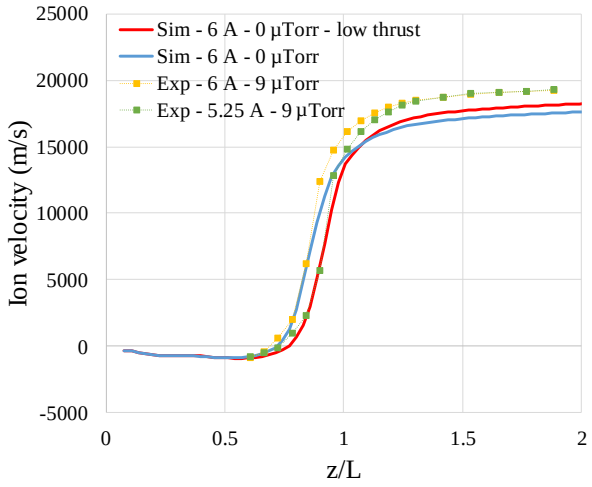

Fig. 12. Ion velocity profile along the channel centerline at 4.5 kW, 6 A magnet current from the simulation without axial shift in the acceleration region between vacuum and 9 µTorr and the "low thrust" simulation in which the acceleration region in vacuum was shifted downstream. The LIF measurements at 9 µTorr for the 5.25-A and 6-A magnet current conditions are also included for reference.

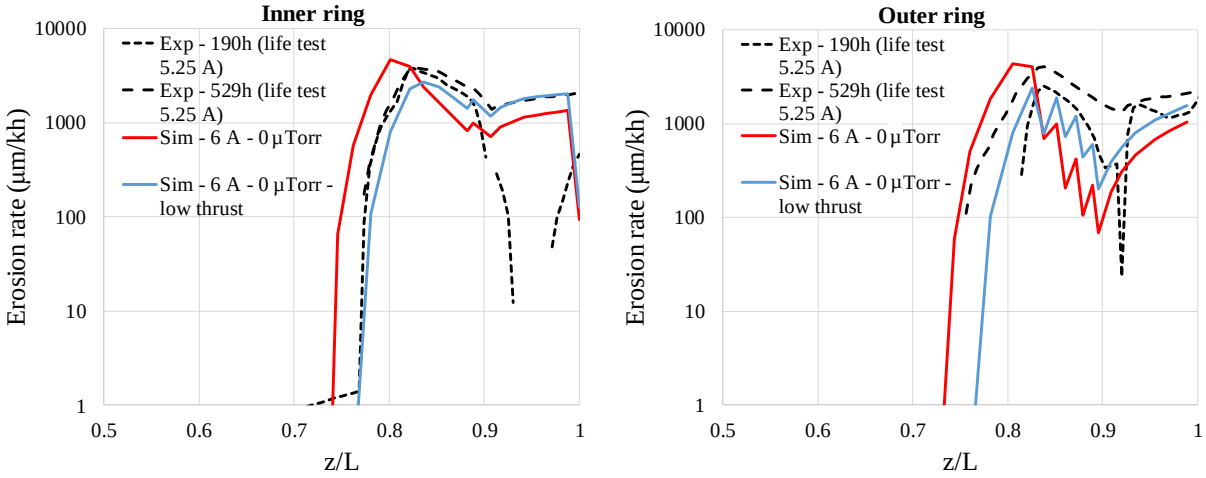

Fig. 13. Erosion rates at the inner and outer rings predicted at vacuum from the original simulation (LIF-

informed) and the "low thrust" simulation. The erosion rates at beginning of life from the wear test (note magnet current of 5.25 A) are included for reference.

V. Conclusion

We employed the 2-D axisymmetric code Hall2De to conduct numerical simulations of the SPT-140, a Hall thruster that operates with an external cathode. The numerical simulations were informed by direct measurements of the plasma conditions in the acceleration channel that were obtained using LIF diagnostics. These measurements allowed us to define in the simulations the location of the acceleration region as a function of operating condition and background pressure. We validated our simulation results with additional measurements of the plasma properties, erosion rates from ground wear tests, and of the performance as a function of background pressure.

The comparisons of the simulation results with thrust measurements provided insight into the longstanding question of how background pressure affects Hall thruster performance. We found that in thrusters with an external cathode, when the location of the acceleration region is fixed, changes in the thrust with varying backpressure are, in part, due to the changes in the plasma density near the cathode. By invoking Boltzmann's law for the plasma potential, we argued that such changes in the density affect the voltage coupling and, eventually, the thrust. However, this mechanism alone was not enough to explain all the features observed in the computed and measured trends, a topic that is discussed in more detail in our companion article [27]. Of critical importance to our ability to predict thruster behavior during spaceflight have been the trends at the lowest facility backpressures. Here our simulations over-predicted the thrust measured during ground tests. Also, the measurements showed a higher rate of change of the thrust at these pressures compared to the simulations. We proposed that one explanation for this discrepancy is that the acceleration region may be axially shifting downstream with decreasing backpressure. Though possible, we also recognized however that since such shifts were not observed in LIF measurements at the lowest pressures (for which such diagnostics were possible), the mechanism(s) that would cause such movements in vacuum was/were not clear. As such we proposed alternative explanations that are the topic of our companion article [27].

Acknowledgments

The research described in this paper was carried out by the Jet Propulsion Laboratory, California Institute of Technology, under a contract with the National Aeronautics and Space Administration.

References

[1] Snyder, J. S., Lenguito, G., Frieman, J. D., Haag, T. W., and Mackey, J. A., "The Effects of Background Pressure on SPT-140 Hall Thruster Performance", AIAA 2018-4421, 54th Joint Propulsion Conference, Cincinnati, OH, July 2018

[2] Diamant, K.D., Liang R., and Corey, R. L., "The Effect of Background Pressure on SPT-100 Hall Thruster Performance," AIAA 2014-3710, 50th Joint Propulsion Conference, Cleveland, OH, July 28-30, 2014.

[3] Kamhawi, H., Huang, W., Haag, T. W., Yim, J., Herman, D. A., Peterson, P. Y., Williams, G., Gilland, J., Hofer, R. R., and Mikellides, I. G., "Performance, Facility Pressure Effects, and Stability Characterization Tests of NASA's Hall Effect Rocket with Magnetic Shielding Thruster," AIAA 2016-4826, 52nd Joint Propulsion Conference, Salt Lake City, UT, July 25-27, 2016.

[4] Huang, W., Kamhawi, H., and Haag, T. W., "Effect of Background Pressure on the Performance and Plume of the HiVHAc Hall Thruster," IEPC 2013-058, 33rd International Electric Propulsion Conference, Washington, DC, Oct. 6-10, 2013.

[5] Hofer, R.R. and Anderson, J. R., "Finite Pressure Effects in Magnetically Shielded Hall Thrusters," AIAA 2014-3709, 50th Joint Propulsion Conference, Cleveland, OH, July 28-30, 2014.

[6] Byers, D. and Dankanich, J. W., "A Review of Facility Effects on Hall Effect Thrusters," IEPC 2009-076, 31st International Electric Propulsion Conference, Ann Arbor, MI, Sept. 20-24, 2009.

[7] Diamant, K.D., Spektor, R., Beiting, E. J., Young, J. A., and Curtiss, T. J., "The Effects of Background Pressure on Hall Thruster Operation," AIAA 2012-3735, 48th Joint Propulsion Conference, Atlanta, GA, July 30 - Aug. 1, 2012.

[8] Hofer, R. R., Polk, J. E., Sekerak, M. J., Mikellides, I. G., Kamhawi, H., Sarver-Verhey, T. R., Herman, D. A., and Williams, G., "The 12.5-kW Hall Effect Rocket with Magnetic Shielding (HERMeS) for the Asteroid Redirect Robotic Mission", AIAA 2016-4825, 52nd AIAA/SAE/ASEE Joint Propulsion Conference, Salt Lake City, UT, July 2016

[9] Oh, D.Y., Collins, S. M., Goebel, D. M., Hart, W., Lantoine, G., Snyder, J. S., Whiffen, G. J., Elkins-Tanton, L., Lord, P., Pirkl, Z., and Rotlisburger, L., "Development of the Psyche Mission for NASA's Discovery Program," IEPC 2017-153, 35th International Electric Propulsion Conference, Atlanta, GA, Oct. 8-12, 2017.

[10] Hart, W., Brown, G. M., Collins, S. M., De Soria-Santacruz Pich, M., Fieseler, P., Goebel, D. M., Marsh, D., Oh, D. Y., Snyder, J. S., Warner, N., Whiffen, G. J., Elkins-Tanton, L., Bell III, J. F., Lawrence, D. J., Lord, P., and Pirkl, Z.,

"Overview of the Spacecraft Design for the Psyche Mission Concept," IEEE Aerospace Conference, Big Sky, Montana, Mar. 3-10, 2018.

[11] Delgado, J.J., Baldwin, J. A., and Corey, R. L., "Space Systems Loral Electric Propulsion Subsystem: 10 Years of On-Orbit Operation," IEPC 2015-04, 34th International Electric Propulsion Conference, Kobe, Japan, July 6-10, 2015

[12] Jameson-Silva, K., Delgado, J. J., Liang, R., Lord, P. W., Rotlisburger, L., Torres, M., Tomescu, B., Malone, S. P., Werner, E., and Waranauskas, J., "Adaptability of the SSL Electric Propulsion-140 Subsystem for use on a NASA Discovery Class Missions: Psyche," IEPC 2017-181, 35th International Electric Propulsion Conference, Atlanta, GA, Oct. 8-12, 2017.

[13] Delgado, J.J., Corey, R. L., Murashko, V M., Koryakin, A. I., and Pridannikov, S. Y., "Qualification of the SPT-140 for use on Western Spacecraft," AIAA 2014-3606, 50th Joint Propulsion Conference, Cleveland, OH, July 28-30, 2014.

[14] Snyder, J.S. and Hofer, R. R., "Throttled Performance of the SPT-140 Hall Thruster," AIAA 2014-3816, 50th Joint Propulsion Conference, Cleveland, OH, July 28-30, 2014.

[15] Garner, C.E., Jorns, B. A., van Derventer, S., Hofer, R .R., Rickard, R., Liang, R., and Delgado, J. J., "Low-Power Operation and Plasma Characterization of a Qualification Model SPT-140 Hall Thruster for NASA Science Missions," AIAA 2015-3720, 51st Joint Propulsion Conference, Orlando, FL, July 27-29, 2015.

[16] Mikellides, I. G. and Katz, I., "Numerical Simulations of Hall-effect Plasma Accelerators on a Magnetic-Field-Aligned Mesh", Physical Review E, Vol. 86, 2012, p. 046703, doi: 10.1103/PhysRevE.86.046703

[17] Lopez Ortega, A. and Mikellides, I. G., "The Importance of the Cathode Plume and its Interactions with the Ion Beam in Numerical Simulations of Hall Thrusters", *Physics of Plasmas*, Vol. 23, 043515, 2016, doi: 10.1063/1.4947554

[18] Mikellides, I. G., Katz, I., and Hofer, R. R., "Design of a Laboratory Hall Thruster with Magnetically Shielded Walls, Phase I: Numerical Simulations, AIAA 2011-5809, July 2011

[19] Mikellides, I. G., Katz, I., Hofer, R. R., Goebel, D. M., de Grys, K., and Mathers, A., "Magnetic Shielding of the Channel Walls in a Hall Plasma Accelerator", Physics of Plasmas, Vol. 18, 033501, 2011, doi:10.1063/1.3551583

[20] Mikellides, I.G., Katz, I, Hofer, R.R, and Goebel, D. M., "Magnetic Shielding of a Laboratory Hall Thruster, I, Theory and Validation", Journal of Applied Physics, Vol. 115, 043303, 2014, doi: 10.1063/1.4862313

[21] Lopez Ortega, A. and Mikellides, I. G., "A new cell-centered implicit numerical scheme for ions in the 2-D axisymmetric code Hall2De", AIAA paper 2014-3621, in proceedings of the 50th AIAA Joint Propulsion Conference, Cleveland, OH, 2014.

[22] Lopez Ortega, A., Jorns, B. A., Mikellides, I. G., and Hofer, R. R., "Numerical Simulations of the XR-5 Hall thruster for the assessment of erosion rates at different operating conditions" AIAA 2015-4008, 51st Joint Propulsion Conference, Orlando, FL, July 2015

[23] Lopez Ortega, A., Mikellides, I. G., and Chaplin, V. H., "Numerical Simulations for the Assessment of Erosion in the 12.5-kW Hall Effect Rocket with Magnetic Shielding", IEPC 2017-154, 35th International Electric Propulsion Conference, Atlanta, GA, October 2017

[24] Lopez Ortega, A, Mikellides, I. G., Sekerak, M. J, and Jorns, B. A., "Plasma Simulations in 2-D (r-z) Geometry for the Assessment of Pole Erosion in a Magnetically Shielded Hall Thruster", Journal of Applied Physics, Vol. 125, 033302, 2019, doi:10.1063/1.5077097

[25] Cedolin, R. J., Hargus, W. A., Storm, P. V, Hanson, R. K., and Cappelli, M. A., "Laser-Induced Fluorescence Study of a Xenon Hall Thruster", Applied Physics B, Vol. 65, Issue 4-5, pp. 459-469, 1997, doi: 10.1007/s003400050297

[26] Hargus, W. A., and Cappelli, M. A., "Laser-Induced Fluorescence Measurements of Velocity within a Hall Discharge", *Applied Physics B*, Vol. 72, Issue 8, pp 961-969, 2001, doi: 10.1007/s003400100589

[27] Mikellides, I. G., Lopez Ortega, A., Chaplin, V. H., Snyder, J. S., and Lenguito, G., Facility Pressure Effects on a Hall Thruster with an External Cathode, I: Theoretical Model of the Thrust, *submitted to Plasma Sources Science and Technology concurrently with this article*

[28] Katz, I. and Mikellides, I. G., "Neutral gas free molecular flow algorithm including ionization and walls for use in plasma simulations", *Journal of Computational Physics*, Vol. 230, 2011, pp. 1454-1464, doi: 10.1016/j.jcp.2010.11.013

[29] Hobbs, G. D., and Wesson, J. A., "Heat Flow through a Langmuir Sheath in Presence of Electron Emission," *Plasma Physics*, vol. 9, no. 1, pp. 85-87, 1967, doi: 10.1088/0032-1028/9/1/410

[30] Mikellides, I. G., Katz, I., Goebel, D. M., Jameson, K. K. and Polk, J. E., "Wear Mechanisms in Electron Sources for Ion Propulsion II: Discharge Hollow Cathodes", *Journal of Propulsion of Power*, Vol. 24, No 4, 2008, 866-879, doi: 10.2514/1.33462

[31] Mikellides, I. G., Katz, I., D. Goebel, D. M., and Polk, J. E., "Hollow Cathode Theory and Experiment II: A Two-dimensional Theoretical Model of the Emitter Region", *Journal of Applied Physics*, Vol. 98, No. 11, 2005, 113303, doi: 10.1063/1.2135409

[32] Mikellides, I. G, Katz, I., Jameson, K. K., and Goebel, D. M., "Numerical Simulations of a Hall Thruster Hollow Cathode Plasma", IEPC-2015-018, in proceedings of the 30th International Electric Propulsion Conference, Florence, Italy, September 2007.

[33] Mikellides, I. G., Katz, I., Goebel, D. M., Polk, J. E., and Jameson, K. K., "Evidence of Non-classical Plasma Transport in Hollow Cathodes for Electric Propulsion", *Journal of Applied Physics*, Vol. 101, No. 6, 2007, 063301, doi: 10.1063/1.2710763

[34] Mikellides, I. G. and Katz, I., "Wear Mechanisms in Electron Sources for Ion Propulsion I: Neutralizer Hollow Cathode", *Journal of Propulsion and Power*, Vol. 24, No. 4, 2008, 855-865, doi: 10.2514/1.33461

[35] Mikellides, I. G., Goebel, D. M., Jorns, B. A., Polk, J. E., and Guerrero, P., "Numerical Simulations of the Partially-ionized Gas in a 100-A LaB6 Hollow Cathode", *IEEE Transactions on Plasma Science, Special Issue on Plasma Propulsion*, Vol. 43, No. 1, 2015, pp. 173-184, doi: 10.1109/TPS.2014.2320876

[36] Mikellides, I. G., "Effects of Viscosity in a Partially-Ionized Channel Flow with Thermionic Emission," *Physics of Plasmas*, Vol. 16, No. 1, 2009, pp. 013501 (1-10), doi: 10.1063/1.3056397

[37] Mikellides, I. G., and Lopez Ortega, A., "Challenges in the Development and Verification of First-Principles Models in Hall-Effect Thruster Simulations that are based on Anomalous Resistivity and Generalized Ohm's Law", Plasma Sources Science and Technology, Vol. 28, No. 1, 014003, doi:10.1088/1361-6595/aae63b

[38] Bohdansky, J., Roth, J., and Bay, H. L., "An analytical formula and important parameters for low-energy ion sputtering", Journal of Applied Physics, Vol. 51, 1980, p. 1610

[39] Yalin, A. P., Rubin, B., Dominguez, S. R., Glueckert, Z., and Williams, J. D., "Differential sputter yields of boron nitride, quartz and kapton due to low energy Xe+ bombardment", AIAA 2007-5314, 43rd Joint Propulsion Conference, Cincinnati, OH, 2007

[40] Hofer, R. R., Mikellides, I. G., Katz, I., and Goebel, D. M., "Wall Sheath and Electron Mobility Modeling in Hybrid-PIC Hall Thruster Simulations" AIAA 2007-5267, 43rd Joint Propulsion Conference, Cincinnati, OH, July 2007

[41] Raitses, Y., Dourbal, P., Spektor, R., "Secondary Electron Emission Properties of Boron Nitride Ceramic Materials at High Temperatures", IEPC 2015-342, 34th International Electric Propulsion Conference, Kobe, Japan, July 2015

[42] Heron, A., and Adam, J. C., "Anomalous Conductivity in Hall Thrusters: Effects of the Non-linear Coupling of the Electron-Cyclotron Drift Instability with Secondary Electron Emission of the Walls", Physics of Plasmas, Vol. 20, 082313, 2013, doi: 10.1063/1.4818796

[43] Adam, J. C., Heron, A., and Laval, G., "Study of Stationary Plasma Thrusters Using Two-dimensional Fully Kinetic Simulations", Physics of Plasmas, Vol. 11, 2004, 295, doi: 10.1063/1.1632904